Journal of Materials Chemistry A

ROYAL SOCIETY OF CHEMISTRY

PAPER

View Article Online
View Journal | View Issue

Cite this: J. Mater. Chem. A, 2023, 11, 16172

Constructing atomic single metal Co–$C_3(OH)_1$ sites with graphdiyne for zinc–air batteries†

Meiping Li,[a] Zhufeng Hou,[b] Xiaodong Li,[c] Changshui Huang[c] and Qing Lv *[a]

Single-atom metal–N_x sites have exhibited excellent catalytic properties and garnered growing attention. Typically, these metal atoms rely heavily on N atoms to anchor them to the carbon substrate. However, since N atoms are generally doped by post-treatments, the content of N is low. Thus, it is limited in constructing diverse efficient single-atom active sites. Herein, we employ hydrogen-substituted graphdiyne (HsGDY) as a carbon substrate to construct a cobalt atom electrocatalyst (Co-HsGDY) for the oxygen reduction reaction (ORR). Thanks to the special sp-C in HsGDY, Co atoms can be anchored to the carbon support without the help of N. Besides, benefitting from the elegant molecular pores of HsGDY, there is enough space for the metal atoms to coordinate with oxygen-containing groups, which further modulates the electronic structure of the central metal. The Co-HsGDY exhibits an ORR catalytic activity comparable to that of Pt/C. Moreover, the Co-HsGDY based rechargeable zinc–air battery displays an outstanding performance with a power density as high as 209.5 mW cm^{-2} and superior long-term stability.

Received 21st April 2023
Accepted 30th June 2023

DOI: 10.1039/d3ta02386a

rsc.li/materials-a

[a]Shandong Provincial Key Laboratory for Science of Material Creation and Energy Conversion, Science Center for Material Creation and Energy Conversion, School of Chemistry and Chemical Engineering, Shandong University, Jinan 250100, P. R. China. E-mail: lvqing@sdu.edu.cn

[b]State Key Laboratory of Structural Chemistry, Fujian Institute of Research on the Structure of Matter, Chinese Academy of Sciences, Fuzhou 350002, P. R. China

[c]Institute of Chemistry, Chinese Academy of Science, Zhongguancun North First Street 2, Beijing 100191, P. R. China

† Electronic supplementary information (ESI) available. See DOI: https://doi.org/10.1039/d3ta02386a

Qing Lv is an associate professor of the Science Center for Material Creation and Energy Conversion, School of Chemistry and Chemical Engineering, Shandong University. She received a PhD degree in Physical Chemistry from Changchun Institute of Applied Chemistry (CIAC), Chinese Academy of Sciences (CAS) in 2016. Then she worked in Prof. Changshui Huang's group from 2016 to 2020 at Qingdao Institute of Bioenergy and Bioprocess Technology (QIBEBT), CAS, as a postdoctoral fellow, assistant professor and associate professor, successively. Her current research is focused on the design and synthesis of graphdiyne-based materials for electrocatalysis applications.

Introduction

With the aggravation of environmental pollution and increasing demand for clean energy, rechargeable zinc–air batteries (ZABs) have aroused great attention and considerable research due to their low cost, eco-friendliness, high energy density, and so on.[1–4] However, the oxygen reduction reaction (ORR) that occurs at the ZAB cathode is a sluggish kinetic process,[5,6] which traditionally relies on expensive platinum.[7] Pt-based catalysts are considered as excellent ORR catalysts owing to their high electrocatalytic activity for the ORR, but the high cost and scarcity of Pt severely hamper the broad commercialization of ZABs.[8] Consequently, it is of great significance to exploit highly efficient and cost-effective non-precious metal electrocatalysts to replace noble Pt-based catalysts.

Recently, emerging as a booming field in heterogeneous catalysis, single-atom catalysts (SACs) have sparked great attention due to their high atom utilization and catalytic performance comparable to those of noble metal catalysts.[9–16] Among them, metal–nitrogen–carbon (M–N–C) moieties, employing nitrogen to anchor dispersed metal atoms to form single atomic sites, exhibit good catalytic activity.[17] Specifically, the widely researched carbon-based SACs with M–N_4 sites have been regarded as burgeoning alternatives to noble Pt-based catalysts.[18] However, it is not easy to create M–N_4 sites, which requires four N atoms to be doped in the immediate vicinity of the carbon substrate precisely. Thus, the doped nitrogen atoms are far more than four times as numerous as metal atoms. Besides, excessive heteroatoms that are not bound to metal atoms will lead to co-existing miscellaneous structures.[19,20]

Accordingly, it is appealing to research new carbon supports to anchor metal atoms without the help of N, and regulate the electronic structure of the central metal by other highly electronegative heteroatoms. It has been demonstrated that Cl and O can downshift the d-band center of some metal atoms efficiently.[21] However, it is difficult to introduce these large-diameter heteroatoms into the traditional graphene-like carbon materials, which needs large vacancy defects, often resulting in poor electroconductivity of the carbon substrates.[22]

Considering the discussion above, hydrogen-substituted graphdiyne (HsGDY), a layered two-dimensional carbon framework, has been studied.[23–25] As for HsGDY, three carbon atoms on the benzene ring are linked to diacetylene chains, while the other three are connected to hydrogen atoms. The novel framework constructs a π-conjugated structure with large molecular pores, which is conducive to electron transfer and mass transfer. Besides, the large molecular pores of HsGDY directly create many internal edge sites similar to the defects formed in graphene, which provides not only available sites to anchor metal atoms but also sufficient space for the coordination of large-diameter heteroatoms, such as Cl and O. Therefore, the unique structure of HsGDY provides more possibilities for the coordination of diverse atoms and the creation of new active sites.

Herein, we propose a strategy to construct Co SACs without the help of nitrogen. Benefitting from the unique structure of HsGDY, the Co atoms can be anchored by sp-C and sp^2-C, and it has available space to coordinate with large-diameter terminal ligands (OH), which further modulates the electronic structure of the central metal. The Co species are atomically dispersed in the as-synthesized catalyst (denoted as Co-HsGDY), which was confirmed by both morphology and structure characterizations. As a result, Co-HsGDY exhibits an ORR activity comparable to that of Pt/C. Besides, the ZAB assembled with Co-HsGDY generates a high power density of 209.5 mW cm^{-2} and superior long-term stability.

Experimental

Materials

Tetrabutylammonium fluoride (TABF), tribromobenzene, and $Pd(PPh_3)_4$ were purchased from Energy Chemical. Cobalt acetylacetonate was bought from Macklin. THF, toluene, pyridine, and copper foil were acquired from Sinopharm Chemical Reagent Co., Ltd.

Synthesis of HsGDY and Co-HsGDY

HsGDY was synthesized according to the methods previously reported,[23,24] but here, it refers to HsGDY annealed at 850 °C under an Ar flow for two hours. A series of catalysts with different Co contents were synthesized, in which the dosages of cobalt acetylacetonate were 1 mg, 3 mg, 5 mg and 7 mg, respectively, denoted as Co-HsGDY-1, Co-HsGDY-2, Co-HsGDY-3, and Co-HsGDY-4, respectively. In detail, HsGDY (15 mg) and cobalt acetylacetonate were dispersed in anhydrous ethanol and stirred overnight. Then, the mixture was washed with an appropriate amount of anhydrous ethanol to remove weakly adsorbed ions and dried in a vacuum oven. Subsequently, the powder was calcined in an Ar atmosphere at 850 °C for 2 h to obtain Co-HsGDY.

Characterization

Scanning electron microscopy (SEM) was conducted with Zeiss Gemini SEM 300 field emission scanning electron microscope. Transmission electron microscopy (TEM) was performed with a Hitachi HT7700 transmission electron microscope. Aberration-corrected high-angle annular dark field scanning transmission electron microscopy (AC HAADF-STEM) and energy dispersive spectroscopy (EDS) mapping were carried out on an FEI-Titan Cubed Themis G2 300 with a spherical aberration corrector. X-ray diffraction (XRD) was carried out on a Japan Rigaku SmartLab 9 kW with a rotating anode X-ray source ($\lambda \sim 1.54$ Å). X-ray photoelectron spectroscopy (XPS) measurements were taken on a Kratos AXIS Supra spectrometer with Al Kα radiation as the excitation source. The X-ray absorption near-edge structure (XANES) spectra analyses were performed at the 4B7A station in the Beijing Synchrotron Radiation Facility.

Electrochemical measurements

All the electrochemical performances were measured on a CHI 760E electrochemical workstation with a conventional three-electrode cell containing O_2-saturated 0.1 M KOH solution. A saturated calomel electrode (SCE) was utilized as a reference electrode. A Pt foil was employed as a counter electrode and the catalyst ink coated RRDE was used as a working electrode. Generally, 5 mg Co-HsGDY was ultrasonically dispersed in a solution of 950 μL ethanol and 50 μL Nafion (5 wt%) to obtain the catalyst ink. Then, the catalyst ink was dispersed on the RRDE with a loading of 0.4 mg cm^{-2} and dried naturally to obtain the electrode coated with catalyst film. All potentials mentioned in this work were calibrated relative to the reversible hydrogen electrode (RHE). The catalytic activities were measured by liner sweep voltammetry (LSV) from 0 V to 1.2 V *vs.* RHE, while the ring electrode was maintained at 1.3 V *vs.* RHE.

Zn–air battery measurements

The zinc–air battery was fabricated by using a fresh zinc sheet as the anode and a carbon paper coated with Co-HsGDY as the cathode. Briefly, the as-prepared catalyst ink was uniformly coated on the carbon paper and freshly prepared 6 M KOH solution was used as the electrolyte. The zinc–air battery assembled with Pt/C was fabricated by the same method. All tests were carried out using the CHI 760E electrochemical workstation and LAND system.

Results

Synthesis and morphology characterization

The synthesis of Co-HsGDY is schematically depicted in Fig. 1a. Firstly, the HsGDY was successfully grown on copper foil by a cross-coupling reaction. To synthesize Co-HsGDY, Co atoms

were separated in HsGDY and subsequently heat-treated in an Ar atmosphere. It can be seen that there are abundant molecular pores in HsGDY, which plays a certain role in the dispersion of the precursor molecules. Additionally, the elegant molecular pores in HsGDY provide a rich internal edge-like structure, which facilitates the creation of active sites. The morphologies of the as-synthesized catalysts were monitored by SEM and TEM. As shown in Fig. 1b and c, Co-HsGDY maintains the same porous structure as HsGDY (Fig. S1†). In addition, no distinct Co nanoparticles can be observed in the TEM images (Fig. 1d), which is further confirmed by the XRD pattern without the diffraction peaks of Co species (Fig. S5†), indicating that Co species may be highly atomically dispersed. The high-resolution TEM images show that the interlayer spacing of Co-HsGDY is around 0.42 nm (Fig. 1e), consistent with the previous reports.[24] Further, AC HAADF-STEM was employed to validate the atomic dispersion of Co species (Fig. 1f and S6†). The bright dots highlighted by yellow cycles represent Co single atoms. Besides, the EDS mapping manifests that Co, C, and O elements are homogeneously distributed in the Co-HsGDY (Fig. 1g). The atomic content of Co in Co-HsGDY is 1.2 wt%, which is determined by inductively coupled plasma-mass spectrometry (ICP-MS).

Coordination structure of atomically dispersed Co sites

In order to disclose the interplay of Co atoms and the carbon matrix in Co-HsGDY, XPS analysis and XANES measurements were performed. As displayed in Fig. 2a, the C 1s spectrum can be well deconvoluted into four peaks, assigned to C–C (sp^2), C–C (sp), C–O, and C=O, respectively. The area ratio of the two hybrid carbons is close to 1 : 1, consistent with HsGDY (Fig. S7†).[23,24] The C K-edge XANES spectra of HsGDY and Co-HsGDY are almost identical (Fig. S9†), which further confirms that their carbon frameworks are consistent. The above results

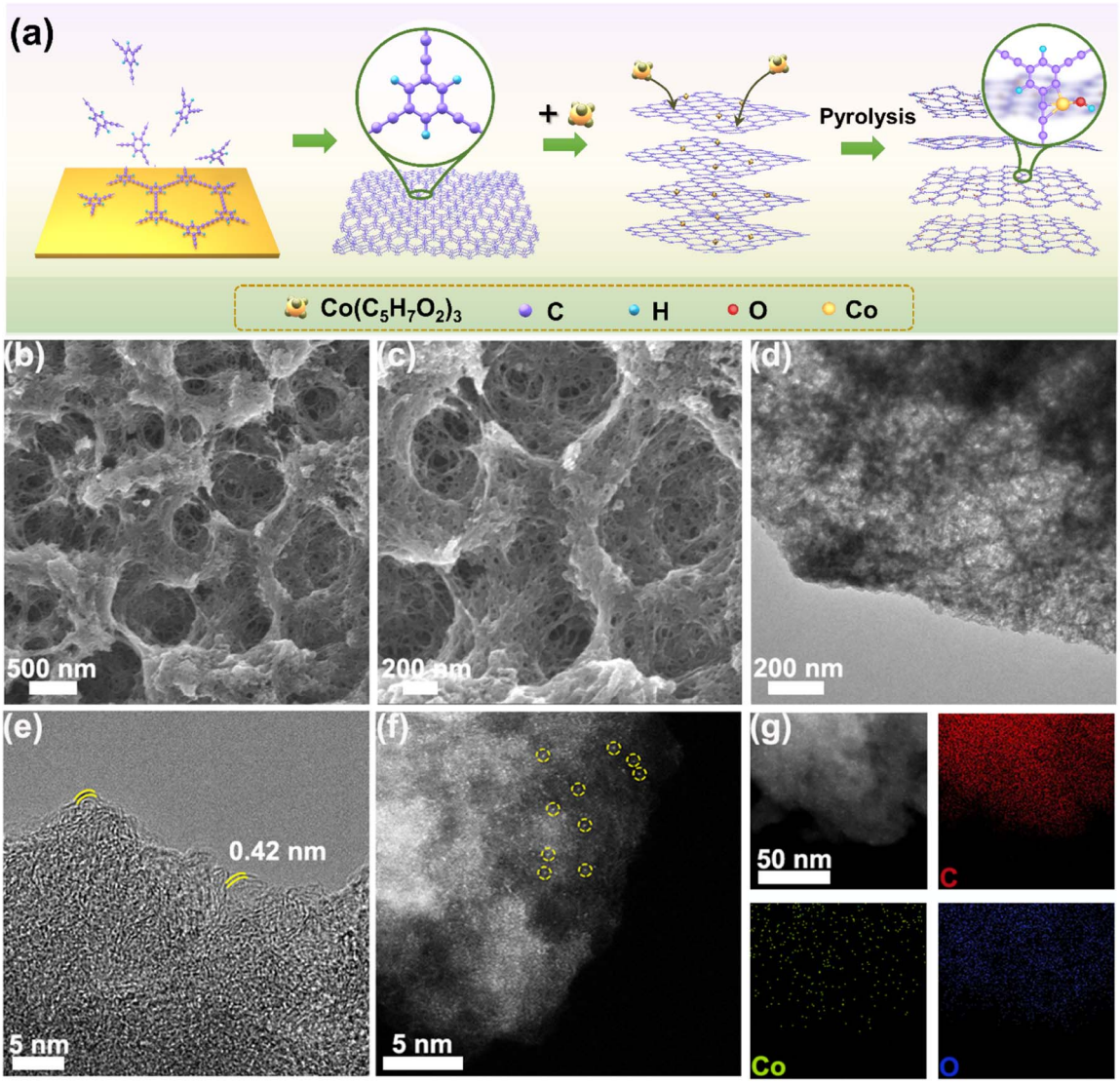

Fig. 1 (a) Synthetic process of Co-HsGDY. (b) Low- and (c) high-magnification SEM images of Co-HsGDY. (d) TEM image and (e) high resolution TEM image of Co-HsGDY. (f) HAADF-STEM image and (g) EDS mapping images of Co-HsGDY.

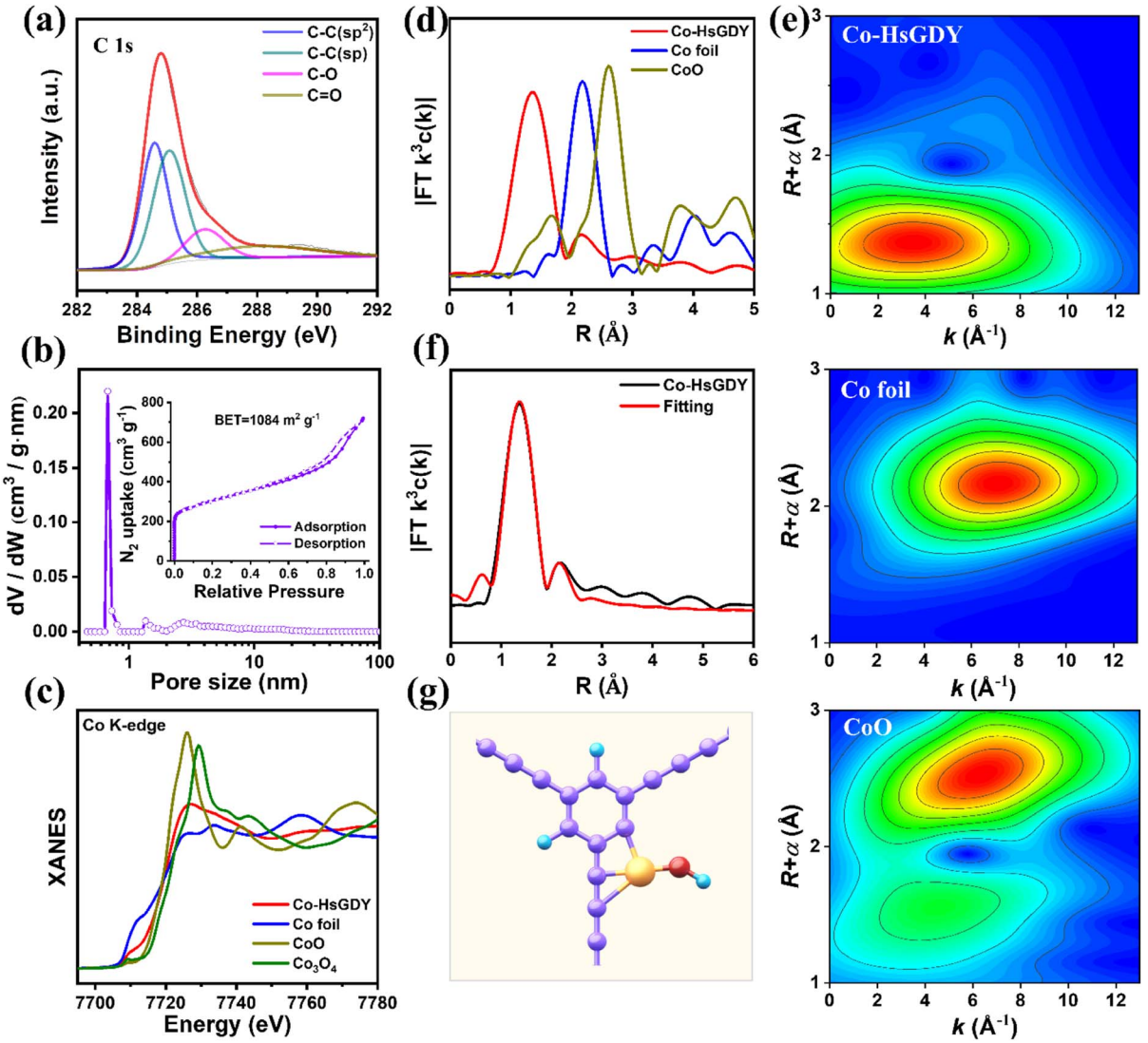

Fig. 2 (a) C 1s XPS spectrum of Co-HsGDY. (b) Pore size distribution curve and N_2 adsorption–desorption isotherm (inset) of Co-HsGDY. (c) Co K-edge XANES spectra and (d) Fourier transform of the EXAFS spectra for Co-HsGDY and the reference samples. (e) Co K-edge WT-EXAFS contour plots of Co foil, CoO, and Co-HsGDY. (f) The corresponding FT-EXAFS fitting curves of Co-HsGDY in *R* space. (g) The schematic model derived from EXAFS.

demonstrate that the structure of HsGDY can be retained after annealing treatment. Additionally, the porous structure of HsGDY was demonstrated by N_2 adsorption–desorption measurement. The surface area of Co-HsGDY is estimated to be as high as 1084 $m^2\ g^{-1}$ (Fig. 2b), which is conducive to the creation as well as exposure of active sites. Meanwhile, the pore size distribution shows a predominance of micropores, but there is a small hysteresis loop in the high pressure region (inset in Fig. 2b), which proves the presence of mesopores and macropores, facilitating the mass transfer during electrochemical processes.

To determine the atomic coordination of Co-HsGDY, X-ray absorption fine structure (XAFS) spectroscopy was conducted at the Co K-edge. As illustrated in Fig. 2c, the absorption edge position of Co-HsGDY situates between CoO and Co_3O_4, indicating that the oxidation state of isolated Co in Co-HsGDY is between +2 and +3. The positive charge of the Co atom stems from the charge transfer from Co to its adjacent C and O atoms, which further regulates the coordination environment of the central metal Co. The Fourier transform extended X-ray absorption fine structure (FT-EXAFS) spectrum of Co-HsGDY exhibits one major peak at 1.36 Å, which is assigned to Co–C and Co–O configurations (Fig. 2d).[26] Meanwhile, the absence of a Co–Co scattering path (2.2 Å) in Co-HsGDY certifies that Co species are atomically dispersed. Furthermore, wavelet transform (WT) EXAFS was employed to discriminate the backscattering atoms due to its high resolution in both *R* and *k* spaces.[27,28] The WT contour plot of Co-HsGDY can be observed with only one distinct intensity maximum at 3.5 $Å^{-1}$, attributed to the Co/C/O contribution (Fig. 2e). The WT contour plot of Co foil exhibits an intensity maximum at approximately 7 $Å^{-1}$, which is ascribed to Co–Co scattering. The above results well

verify the atomic dispersion of Co. The coordination configuration of Co moieties in Co-HsGDY was further investigated by quantitative least-squares. The best-fitting curve and the corresponding extracted fitting EXAFS parameters of Co-HsGDY clearly reveal that the main peak at 1.36 Å could be well interpreted as a Co–O/C contribution (Fig. 2f). The local atomic configuration of the Co center is fitted as $CoC_3(OH)_1$ (Fig. 2g and Table S1†).

ORR performance of atomically dispersed Co-HsGDY

The ORR activities of the Co-HsGDY catalysts were firstly investigated by LSV. As shown in Fig. 3a, the catalytic activity of Co-HsGDY is improved with the increase of the contents of Co in the catalysts, because more single atom active sites are created. However, adding too much Co precursor leads to agglomeration, producing Co nanoparticles (Fig. S4†), which cover the active sites of the catalysts and affect the mass transfer of the ORR, resulting in a degraded catalytic activity. As a compromise, Co-HsGDY-3 (named as Co-HsGDY in other sections) exhibits the highest ORR activity among all the Co-HsGDY catalysts (Fig. 3a). It can be seen that the half-wave potential ($E_{1/2}$) of Co-HsGDY-3 is similar to that of Pt/C (0.83 V), which is also evidenced by a cyclic voltammetry (CV) test. The CV curves of Co-HsGDY and Pt/C were measured in N_2 and O_2-saturated 0.1 M KOH electrolyte, respectively (Fig. S12†). A cathodic ORR peak at 0.81 V is observed for Co-HsGDY comparable to that of Pt/C (0.8 V). The kinetic current density (j_k) of Co-HsGDY is much higher than that of Pt/C recorded at 0.8 V (Fig. 3c), indicating its superior ORR kinetics, which is also confirmed by the smaller Tafel slope (47 *vs.* 75 mV dec^{-1} for Pt/C) (Fig. 3b). In addition, the electrochemical surface areas (ECSAs) were assessed by the double-layer capacitance (C_{dl}) obtained *via* CV measurement. The C_{dl} of Co-HsGDY is 134 mF cm^{-2}, higher than that of bulk HsGDY (98 mF cm^{-2}) (Fig. S13†).

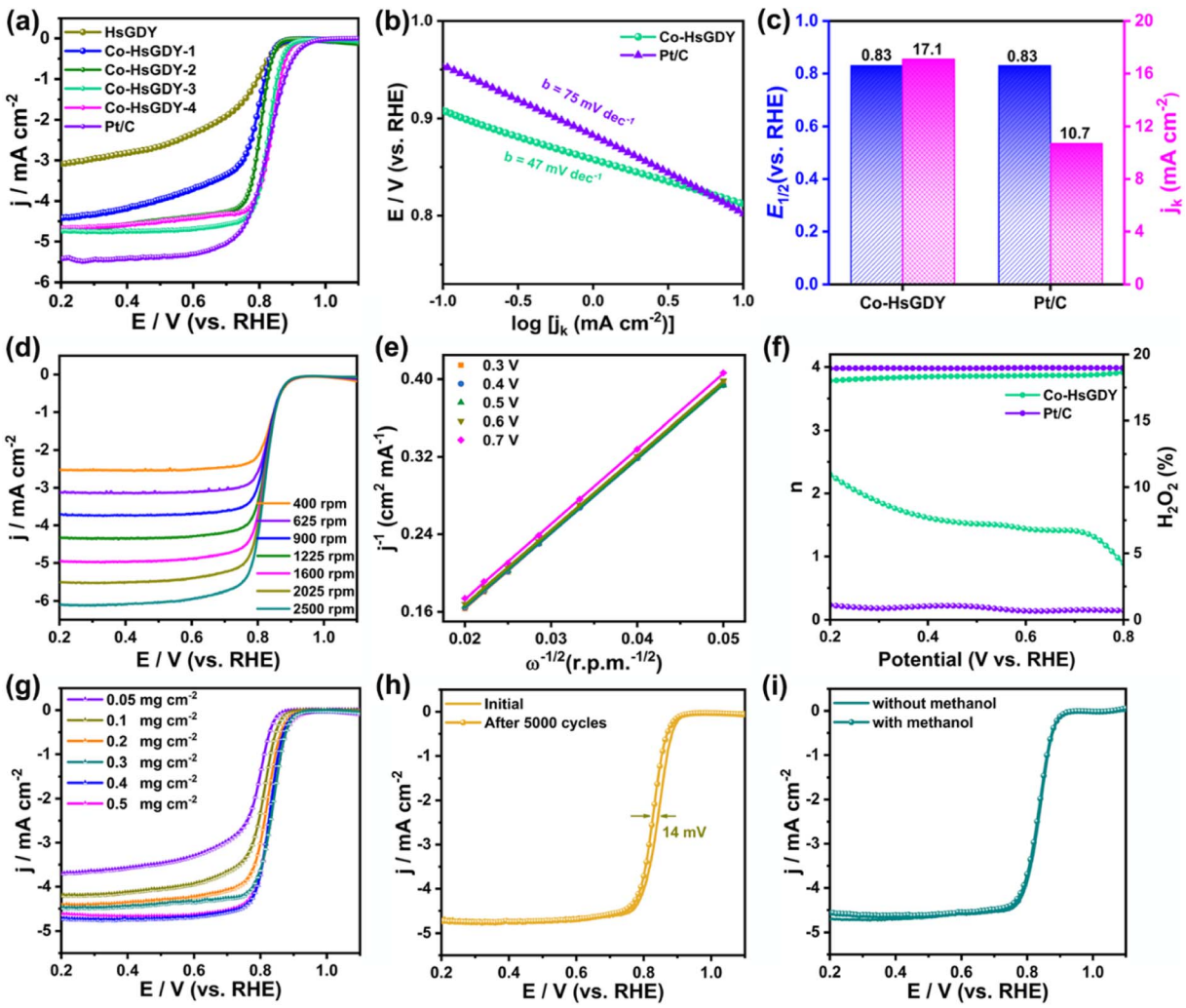

Fig. 3 (a) LSV curves of HsGDY, Co-HsGDY and Pt/C in O_2-saturated 0.1 M KOH at a speed of 1600 rpm. (b) Tafel plots of Co-HsGDY and Pt/C. (c) Kinetic current density (at 0.8 V) and half-wave potential of Co-HsGDY and Pt/C. (d and e) LSV curves at various rotation speeds (d) and the corresponding K–L plots (e) of Co-HsGDY. (f) The electron transfer number and the yield of H_2O_2 for Co-HsGDY obtained using a RRDE. (g) ORR polarization curves of Co-HsGDY with a series of loadings in O_2-saturated 0.1 M KOH. (h and i) Stability test (h) and methanol tolerance (i) of Co-HsGDY.

The large exposed surface area of Co-HsGDY will further facilitate its electrochemical activity. The electrochemical impedance spectroscopy (EIS) plots show that Co-HsGDY exhibits a much smaller charge transfer resistance than HsGDY (Fig. S14†), indicating a fast kinetics process for the ORR. Furthermore, the kinetics of Co-HsGDY was assessed by collecting LSV curves with different rotating speeds varying from 400 to 2500 rpm (Fig. 3d). Based on the Koutecky–Levich (K–L) plots, the electron transfer number of Co-HsGDY is ~3.9 at 0.3–0.7 V, revealing a direct $4e^-$ pathway (Fig. 3e). Meanwhile, the RRDE measurement further confirmed that the ORR process catalyzed by Co-HsGDY mainly undergoes a $4e^-$ electrode process (Fig. 3f). The catalytic activities of Co-HsGDY with different loadings were explored. The Co-HsGDY with loading of 0.4 mg cm^{-2} or 0.5 mg cm^{-2} exhibits the best ORR performance (Fig. 3g). The stability test was conducted by measuring the LSV curves before and after a 5000 cycle CV test (Fig. 3h). The half-wave potential of Co-HsGDY displays a negative shift of 15 mV, while Pt/C shows a larger $E_{1/2}$ shift of 35 mV. Moreover, Co-HsGDY exhibits excellent methanol resistance with negligible shift (Fig. 3i), whereas Pt/C shows an evident methanol oxidation peak (Fig. S15†). Therefore, the atomically dispersed Co-HsGDY exhibits excellent stability and superior methanol tolerance.

Aqueous Zn–air battery performance

Inspired by the highly efficient ORR performance of Co-HsGDY, a home-made Zn–air battery was assembled to investigate its practical application. As schematically illustrated in Fig. 4a, oxygen from the air permeates to the cathode loaded with Co-HsGDY through the waterproof gas-permeable membrane and gets reduced at the interface of the catalyst and electrolyte during the discharge process. A fresh zinc sheet is employed as an anode. The open-circuit voltage (OCV) of the Zn–air battery based on Co-HsGDY is slightly higher than that of Pt/C (1.50 V) (Fig. 4b). An LED bulb can be illuminated with two Co-HsGDY-based ZABs in series (Fig. 4c). The specific capacity of the Co–HsGDY cathode is 739 mA h g^{-1}, surpassing that of the Pt/C

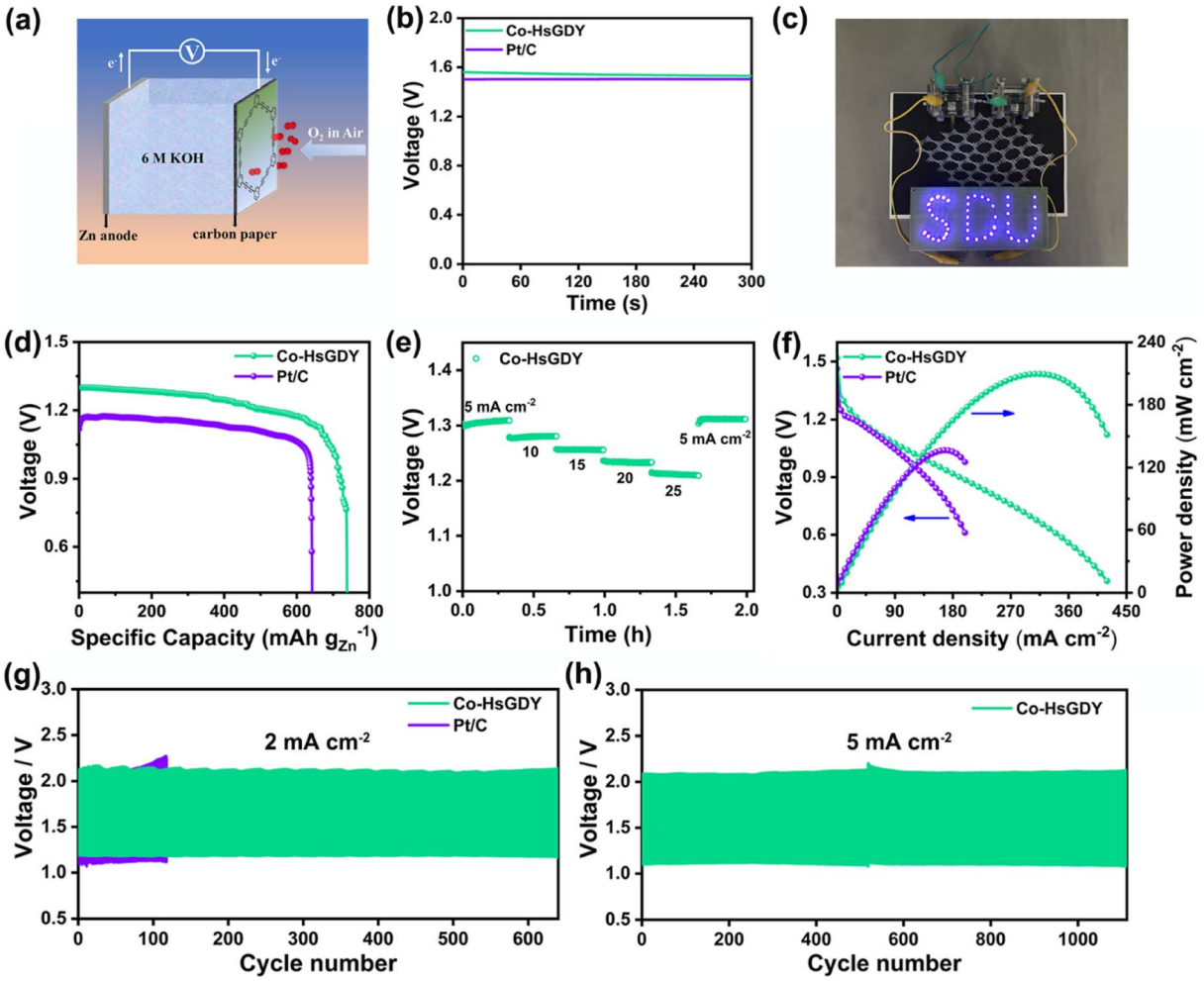

Fig. 4 (a) Schematic model of the homemade Zn–air battery. (b) Open-circuit voltage plots of the liquid ZABs. (c) A photograph of an "SDU"-shaped lamp powered by two Zn–air batteries assembled with Co-HsGDY in series. (d) Specific discharging capacities at 10 mA cm^{-2}. (e) Discharge curves of Co-HsGDY at different current densities. (f) Discharge curves and the corresponding power density curves of ZABs using Co-HsGDY and Pt/C as the air electrode. (g and h) Cycling tests at current densities of 2 mA cm^{-2} and 5 mA cm^{-2}.

cathode (641 mA h g^{-1}), demonstrating a better energy storage capacity (Fig. 4d). The discharge curves of the Co-HsGDY-based ZAB at various current densities were tested (Fig. 4e). Compared with Pt/C (Fig. S16†), Co-HsGDY exhibits a superior rate performance with negligible decay in potential. Remarkably, the ZAB assembled with Co-HsGDY delivers a power density of 209.5 mW cm^{-2}, which is much higher than that of Pt/C (136 mW cm^{-2}, Fig. 4f) and exceeds that of most of the advanced catalysts (Table S3†).[29–31] We conclude that this may be due to the high specific surface area and porous structure of Co-HsGDY, which promotes the charge transfer during charging and discharging. Subsequently, the long-term stability of the assembled liquid Zn–air battery was evaluated. Notably, the Co-HsGDY-based ZAB generates a smaller voltage interval (1.17 V for discharge and 2.13 V for charge) and runs stably up to 640 cycles without obvious voltage attenuation at a current density of 2 mA cm^{-2} (Fig. 4g). By contrast, the Pt/C-based battery exhibits limited cycling capacity and significant voltage decay. Moreover, the Co-HsGDY-based battery can also operate stably for more than 1100 cycles at a high current of 5 mA cm^{-2} (Fig. 4h), which demonstrates that Co-HsGDY is a promising cathode catalyst in Zn–air batteries.

To reveal the underlying mechanism at the atomic level of the high catalytic activity of Co-HsGDY, density functional theory (DFT) calculations were carried out. As the d-band center can reflect the metal–adsorbate interaction, the density of states (DOS) for $CoC_3(OH)_x$ ($x = 0$ and 1) is investigated (Fig. 5a and b). As is well known, the rate-determining step (RDS) for most ORR active sites is the *OH desorption.[32–35] Apparently, when the OH ligand is coordinated with the Co atom, the d-band center displays a downshift, indicating the weakened absorption energy between the Co center and *OH. Additionally, $CoC_3(OH)_1$ presents a larger Bader charge in comparison with CoC_3, suggesting a more obvious charge transfer (Fig. 5c).[36] Subsequently, the linear relationship between the Bader charge of the Co center and the adsorption energy of the *OH ligand is established. As presented in Fig. 5d, with the increase of the Bader charge of the central metal, the adsorption of *OH is weakened, which is conducive to the desorption of *OH, thus improving the ORR activity. In short, the excellent ORR performance of $CoC_3(OH)_1$ originates from the unique structure of HsGDY, whose elegant molecular pores provide enough space for the coordination of large-size groups (OH), further modulating the electronic structure of the central metal.

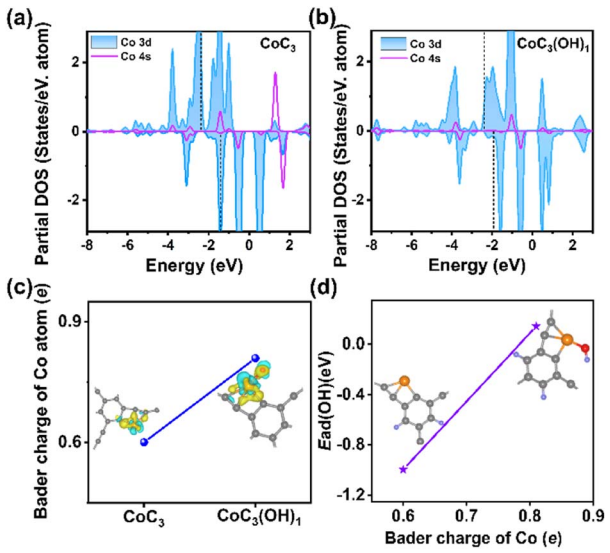

Fig. 5 (a and b) The calculated DOS of the Co site for CoC_3 and $CoC_3(OH)_1$ configurations. (c) The Bader charge of the metal center and the corresponding charge density difference diagram (inset) for CoC_3 and $CoC_3(OH)_1$. (d) Linear relationship between the *OH binding energy and the Bader charge of the metal center. C: grey; O: red; Co: orange; H: lilac.

Conclusion

Taking advantage of the unique structure of HsGDY, a Co SAC without N atom coordination was successfully synthesized. The local atomic structure of the Co center revealed by XANES and EXAFS measurements is the $CoC_3(OH)_1$ moiety. The as-synthesized Co-HsGDY exhibits excellent ORR activity and stability. Additionally, a Zn–air battery was assembled with Co-HsGDY to explore its feasibility in practical applications. Experimental results demonstrate that the Co-HsGDY-based ZAB displays an encouraging power density and superior rate performance, as well as a distinguished cycling stability, which corroborates its promising potential in ZABs. DFT calculations unveil that the coordination of the OH ligand tunes the electronic structure of the Co center, thus enhancing its ORR activity. This finding not only confirms the creation of new ORR active sites, but also provides enlightening guidance for the design of carbon substrates.

Author contributions

M. P. Li performed the synthesis, electrochemical tests, and systematic characterization and co-wrote the paper. X. D. Li and C. S. Huang assisted in analysing the XPS and TEM data. Z. F. Hou conducted computational studies and analysed the computational data. Q. Lv guided the research and co-wrote the paper. All authors discussed the results and commented on the manuscript.

Conflicts of interest

There are no conflicts to declare.

Acknowledgements

This work was supported by the National Natural Science Foundation of China (No. 21790051), the National Key Research and Development Project of China (2022YFA1204500, 2022YFA1204501), the Natural Science Foundation of Shandong Province (ZR2021MB015), the Open Funds of the State Key Laboratory of Electroanalytical Chemistry (SKLEAC202202) and the Young Scholars Program of Shandong University.

References

1 X. Liu, Y. Yuan, J. Liu, B. Liu, X. Chen, J. Ding, X. Han, Y. Deng, C. Zhong and W. Hu, *Nat. Commun.*, 2019, **10**, 4767.
2 M. F. Sanad, A. R. Puente Santiago, S. A. Tolba, M. A. Ahsan, O. Fernandez-Delgado, M. Shawky Adly, E. M. Hashem, M. Mahrous Abodouh, M. S. El-Shall, S. T. Sreenivasan, N. K. Allam and L. Echegoyen, *J. Am. Chem. Soc.*, 2021, **143**, 4064–4073.
3 X. Liu, Y. Zhang, Z. Zhao, H. Gao, J. Kang, R. Wang, G. Ge and X. Jia, *J. Mater. Chem. A*, 2021, **9**, 22643–22652.
4 W. Sun, F. Wang, B. Zhang, M. Zhang, V. Küpers, X. Ji, C. Theile, P. Bieker, K. Xu and C. Wang, *Science*, 2021, **371**, 46–51.
5 R. Jiang, L. Li, T. Sheng, G. Hu, Y. Chen and L. Wang, *J. Am. Chem. Soc.*, 2018, **140**, 11594–11598.
6 M. Li, Q. Lv, W. Si, Z. Hou and C. Huang, *Angew. Chem., Int. Ed.*, 2022, **61**, e202208238.
7 M. Li, K. Duanmu, C. Wan, T. Cheng, L. Zhang, S. Dai, W. Chen, Z. Zhao, P. Li, H. Fei, Y. Zhu, R. Yu, J. Luo, K. Zang, Z. Lin, M. Ding, J. Huang, H. Sun, J. Guo, X. Pan, W. A. Goddard, P. Sautet, Y. Huang and X. Duan, *Nat. Catal.*, 2019, **2**, 495–503.
8 X. Wan, X. Liu, Y. Li, R. Yu, L. Zheng, W. Yan, H. Wang, M. Xu and J. Shui, *Nat. Catal.*, 2019, **2**, 259–268.
9 M. Zhao, H. Liu, H. Zhang, W. Chen, H. Sun, Z. Wang, B. Zhang, L. Song, Y. Yang, C. Ma, Y. Han and W. Huang, *Energy Environ. Sci.*, 2021, **14**, 6455–6463.
10 L. Han, H. Cheng, W. Liu, H. Li, P. Ou, R. Lin, H.-T. Wang, C.-W. Pao, A. R. Head, C.-H. Wang, X. Tong, C.-J. Sun, W.-F. Pong, J. Luo, J.-C. Zheng and H. L. Xin, *Nat. Mater.*, 2022, **21**, 681–688.
11 Y. Liu, X. Liu, Z. Lv, R. Liu, L. Li, J. Wang, W. Yang, X. Jiang, X. Feng and B. Wang, *Angew. Chem., Int. Ed.*, 2022, **134**, e202117617.
12 R. Zhao, Z. Chen, Q. Li, X. Wang, Y. Tang, G. Fu, H. Li, J.-M. Lee and S. Huang, *Chem Catal.*, 2022, **2**, 3590–3606.
13 J. Chen, H. Li, C. Fan, Q. Meng, Y. Tang, X. Qiu, G. Fu and T. Ma, *Adv. Mater.*, 2020, **32**, 2003134.
14 C. Fan, X. Wang, X. Wu, Y. Chen, Z. Wang, M. Li, D. Sun, Y. Tang and G. Fu, *Adv. Energy Mater.*, 2023, **13**, 2203224.
15 X. Wang, J. Wang, P. Wang, L. Li, X. Zhang, D. Sun, Y. Li, Y. Tang, Y. Wang and G. Fu, *Adv. Mater.*, 2022, **34**, 2206540.
16 X. Wang, M. Li, P. Wang, D. Sun, L. Ding, H. Li, Y. Tang and G. Fu, *Small Methods*, 2023, 2300100.
17 C.-X. Zhao, J.-N. Liu, J. Wang, D. Ren, B.-Q. Li and Q. Zhang, *Chem. Soc. Rev.*, 2021, **50**, 7745–7778.
18 L. Jiao, J. Li, L. L. Richard, Q. Sun, T. Stracensky, E. Liu, M. T. Sougrati, Z. Zhao, F. Yang, S. Zhong, H. Xu, S. Mukerjee, Y. Huang, D. A. Cullen, J. H. Park, M. Ferrandon, D. J. Myers, F. Jaouen and Q. Jia, *Nat. Mater.*, 2021, **20**, 1385–1391.
19 J. Hu, W. Shang, C. Xin, J. Guo, X. Cheng, S. Zhang, S. Song, W. Liu, F. Ju, J. Hou and Y. Shi, *Angew. Chem., Int. Ed.*, 2023, e202304754.
20 M. Xiao, Z. Xing, Z. Jin, C. Liu, J. Ge, J. Zhu, Y. Wang, X. Zhao and Z. Chen, *Adv. Mater.*, 2020, **32**, 2004900.
21 M. Xiao, Y. Chen, J. Zhu, H. Zhang, X. Zhao, L. Gao, X. Wang, J. Zhao, J. Ge, Z. Jiang, S. Chen, C. Liu and W. Xing, *J. Am. Chem. Soc.*, 2019, **141**, 17763–17770.
22 L. Dai, Y. Xue, L. Qu, H. J. Choi and J. B. Baek, *Chem. Rev.*, 2015, **115**, 4823–4892.
23 J. He, N. Wang, Z. Cui, H. Du, L. Fu, C. Huang, Z. Yang, X. Shen, Y. Yi, Z. Tu and Y. Li, *Nat. Commun.*, 2017, **8**, 1172.
24 Q. Lv, W. Si, J. He, L. Sun, C. Zhang, N. Wang, Z. Yang, X. Li, X. Wang, W. Deng, Y. Long, C. Huang and Y. Li, *Nat. Commun.*, 2018, **9**, 3376.
25 H. Wei, R. Shi, L. Sun, H. Yu, J. Gong, C. Liu, Z. Xu, Y. Ni, J. Xu and W. Xu, *Nat. Commun.*, 2021, **12**, 1068.
26 J. Chen, H. Li, C. Fan, Q. Meng, Y. Tang, X. Qiu, G. Fu and T. Ma, *Adv. Mater.*, 2020, **32**, 2003134.
27 H. Fei, J. Dong, M. J. Arellano-Jimenez, G. Ye, N. Dong Kim, E. L. Samuel, Z. Peng, Z. Zhu, F. Qin, J. Bao, M. J. Yacaman, P. M. Ajayan, D. Chen and J. M. Tour, *Nat. Commun.*, 2015, **6**, 8668.
28 H. Shang, W. Sun, R. Sui, J. Pei, L. Zheng, J. Dong, Z. Jiang, D. Zhou, Z. Zhuang, W. Chen, J. Zhang, D. Wang and Y. Li, *Nano Lett.*, 2020, **20**, 5443–5450.
29 Y. Zheng, S. Chen, K. A. I. Zhang, J. Zhu, J. Xu, C. Zhang and T. Liu, *ACS Appl. Mater. Interfaces*, 2021, **13**, 13328–13337.
30 C.-C. Weng, J.-T. Ren, H.-Y. Wang, X.-W. Lv, Y.-J. Song, Y.-S. Wang, L. Chen, W.-W. Tian and Z.-Y. Yuan, *Appl. Catal., B*, 2022, **307**, 121190.
31 Q. Zhou, S. Hou, Y. Cheng, R. Sun, W. Shen, R. Tian, J. Yang, H. Pang, L. Xu, K. Huang and Y. Tang, *Appl. Catal., B*, 2021, **295**, 120281.
32 T. Cui, Y. P. Wang, T. Ye, J. Wu, Z. Chen, J. Li, Y. Lei, D. Wang and Y. Li, *Angew. Chem., Int. Ed.*, 2022, **61**, e202115219.
33 M. Xiao, L. Gao, Y. Wang, X. Wang, J. Zhu, Z. Jin, C. Liu, H. Chen, G. Li, J. Ge, Q. He, Z. Wu, Z. Chen and W. Xing, *J. Am. Chem. Soc.*, 2019, **141**, 19800–19806.
34 Y. Lin, P. Liu, E. Velasco, G. Yao, Z. Tian, L. Zhang and L. Chen, *Adv. Mater.*, 2019, **31**, 1808193.
35 W. Si, Z. Yang, X. Hu, Q. Lv, X. Li, F. Zhao, J. He and C. Huang, *J. Mater. Chem. A*, 2021, **9**, 14507–14514.
36 Y. Wu, J. Yang, Z. Wang, C. X. Huang, Y. Zhang, Q. Zhang, C. Chen, J. Du, X. Zhou, Y. Zhang, H. Zhou, L. Wang, X. Zheng, L. Gu and L. M. Yang, *Angew. Chem., Int. Ed.*, 2021, **60**, 22722–22728.